

**Electronic supplementary information for**

**Surface hybridization of diamond with vertical graphene: a new  
route to diamond electronics**

K. P. S. S. Hembram<sup>†a</sup>, Sohyung Lee<sup>†ab</sup>, Hyunsik Im<sup>b</sup>, Hyunsu Ju<sup>a</sup>, Sang-Hun Jeong<sup>c</sup> and  
Jae-Kap Lee<sup>a\*</sup>

<sup>a</sup>Center for Opto-electronic Materials and Devices, Korea Institute of Science and  
Technology (KIST), Seoul 02792, South Korea.

<sup>b</sup>Department of Semiconductor Science, Dongguk University, Seoul 04620, South Korea.

<sup>c</sup>Gwangju Center, Korea Basic Science Institute (KBSI), Gwangju 61186, South Korea.

*†These authors contributed equally to this work.*

*\*Corresponding author. Email: [jkleee@kist.re.kr](mailto:jkleee@kist.re.kr) (Jae-Kap Lee)*

**This PDF file includes:**

Materials and Methods

Fig. S1 to S5

Text (Absorption properties)

References

## Materials and Methods

We synthesized graphene layers on  $\langle 110 \rangle$  textured mirror polished CVD diamond plates of  $1 \times 1 \text{ cm}^2$  (0.7 mm in thickness) in direct current plasma CVD chamber<sup>19,21</sup> by a hydrogen plasma treatment for 1 and 10 minutes. The treatment was performed at high temperature of 1300 °C where graphitic phases is stable. The temperature was expected from 1500 °C measured by a pyrometer which is higher by  $\sim 200$  °C than real one due to additional emission from the hot cathode ( $> 2000$  °C), and was controlled by input power. Gas flow and pressure were 200 sccm and 100 Torr, respectively. The *v-Gr*-diamond hybrid structures were analyzed by SEM, AFM, XRD (normal scan, low angle and rocking curve), Raman and photoluminance (PL). The surface morphology was probed by a SEM (Noba Nano 200) and non-contact-mode AFM (PSIA, XE-100). XRD analysis was performed with Rigaku D/MAX 2200V spectrometer using a  $\text{CuK}\alpha$  source. Raman and PL analysis was performed with inVia-Reflex Raman microscope (Time-resolving PL/Raman spectrometer, Renishaw).

The calculations were based on first-principles density functional theory (DFT) as implemented in the QUANTUM ESPRESSO simulation package.<sup>40</sup> We used generalized gradient approximation (GGA)<sup>41</sup> for exchange correlation energy of electrons and ultra-soft pseudo potentials to represent interaction between ionic cores and valence electrons.<sup>42</sup> Kohn-Sham wave functions were represented with a plane-wave basis with an energy cutoff of 40 Ry and a charge density with a cutoff 240 Ry. Integration over irreducible Brillouin zone for charge density and total energy was performed with a uniform mesh of  $4 \times 4 \times 1$  mesh of  $k$  points.<sup>43</sup> Occupation numbers were smeared using Methfessel-Paxton scheme with broadening of 0.01 Ry.<sup>44</sup> Errors in the stress and total energy due to basis-set size, smearing parameter, and  $k$  points are converged to less than 0.03 GPa and  $10^{-6}$  Ry, respectively.

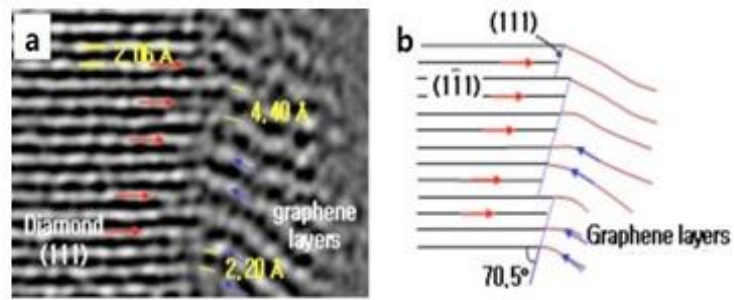


**Fig. S1.** Diamond-graphene interface. a) High resolution transmission electron microscope (HRTEM) image of diamond-graphene interface. b) Schematic showing interface registry based on the HRTEM image. Blue arrows indicate the 1:1 registry, while red arrows indicate internal diamond (111) planes disconnected, thus forming the 2:1 registry (*Permission from ref. 19*).

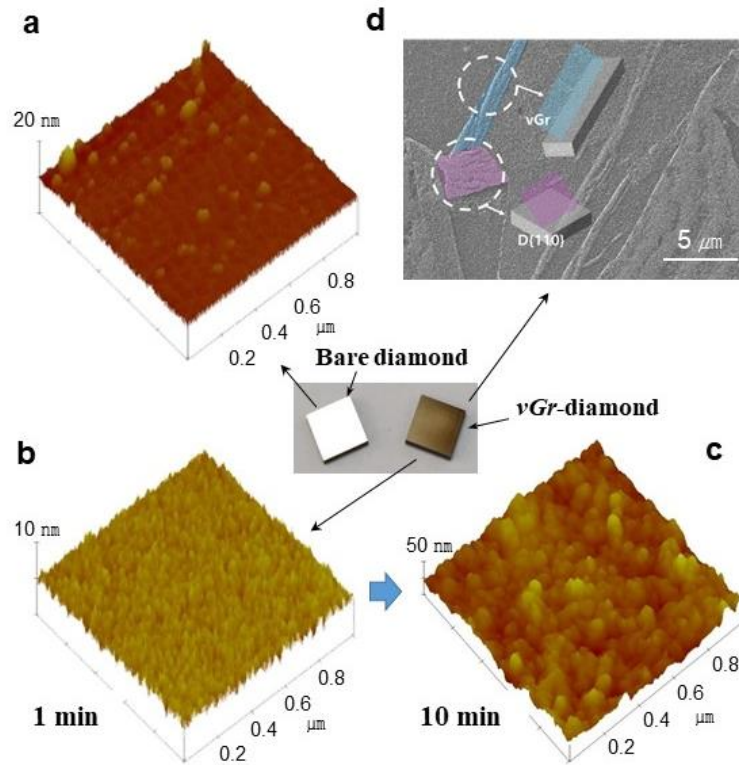


**Fig. S2.** AFM and SEM images for the samples. a) AFM image for bare diamond. b,c) AFM images for *vGr*-diamond where graphene grew for 1 (b) and 10 min (c). Growth rate of graphene is expected to be  $\sim 5$  nm/min. RMS of the hybrid structure (b) is measured to be  $\sim 3$  nm and  $\sim 20$  nm for 1 min and 10 min sample respectively, where the former corresponds to that of the bare surface of mirror polished diamond (a). d) SEM image for the hybrid structure. Schematic explains the graphene layers angled by  $\sim 30^\circ$  to diamond surface at different direction, explaining the unique pattern.

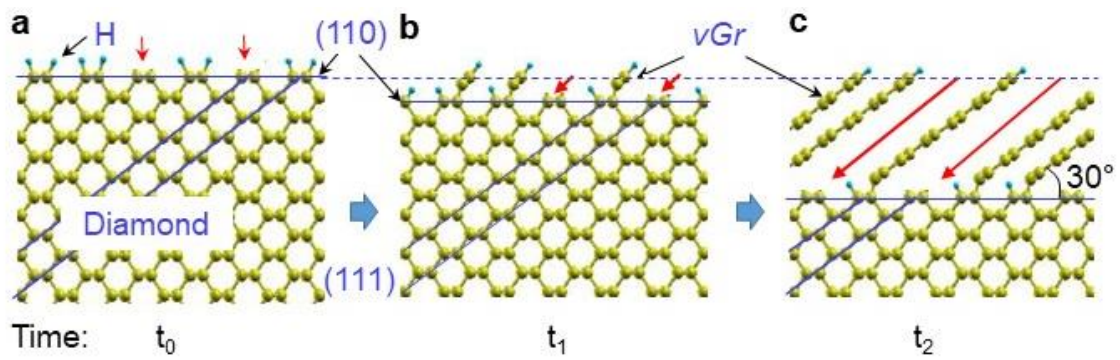


**Fig. S3.** Schematics explaining formation mechanism of *vGr*-diamond hybrid structures on diamond (110) surfaces. a) Atomic model showing hydrogenated diamond (110) surface where each dangling carbon atom is attached with a hydrogen atom (H) (before starting ( $t_0$ ) the transformation of diamond (111) plane to graphene layers). Red arrows indicate carbon atoms where H was detached when temperature is elevated up to the zone (1300 °C) where graphite is stable. b,c) Schematics explaining inward transformation of diamond (111) planes to graphene at 1300 °C under hydrogen plasma, producing the *vGr*-diamond hybrid structures. Solid red arrows in (b,c) indicate inward growth of graphene. Time indicates duration time of plasma treatment ( $t_1 < t_2$ ).

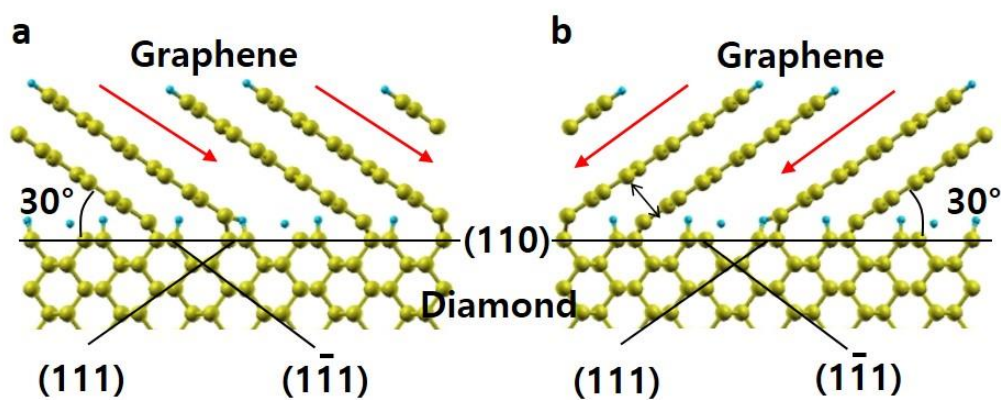


**Fig. S4.** Two examples of epitaxial (etching) growth of graphene layers from diamond (110) surface. Graphene can grow into diamond along different (111) planes of diamond, resulting in the localized graphene structures on diamond surface (the unique SEM pattern). Red arrow indicates direction of the selective etching (Figure 3).

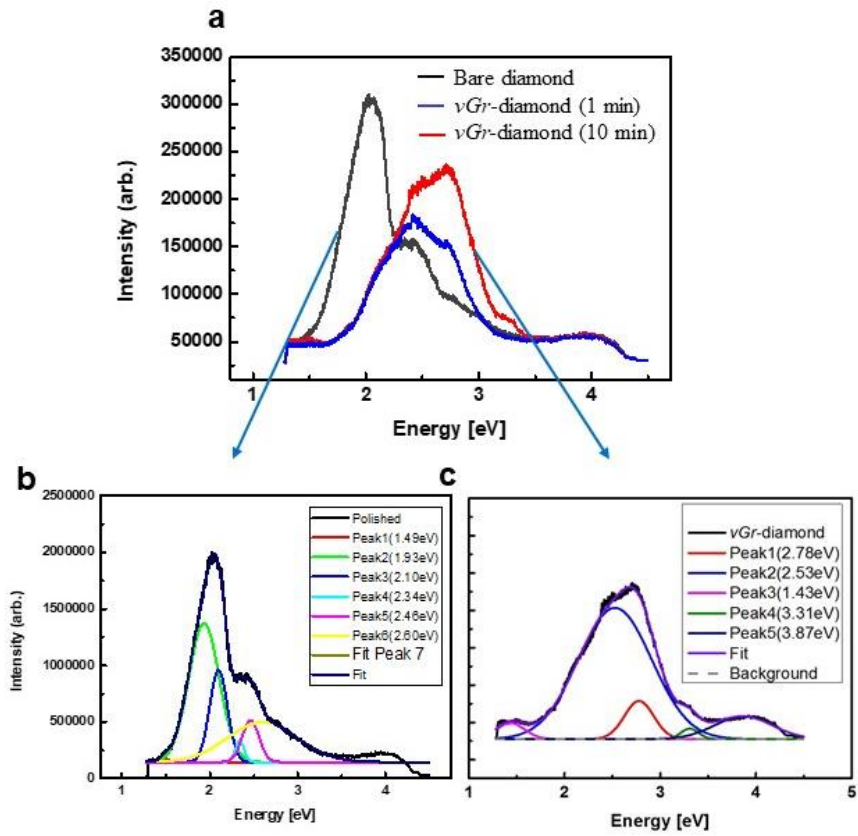


**Fig. S5.** Analysis of PL spectra for the samples, shown in Figure 5a. a) PL spectra for the samples. b,c) Deconvolution of the PL spectra for bare diamond (b) and vGr-diamond (10 min) (c).

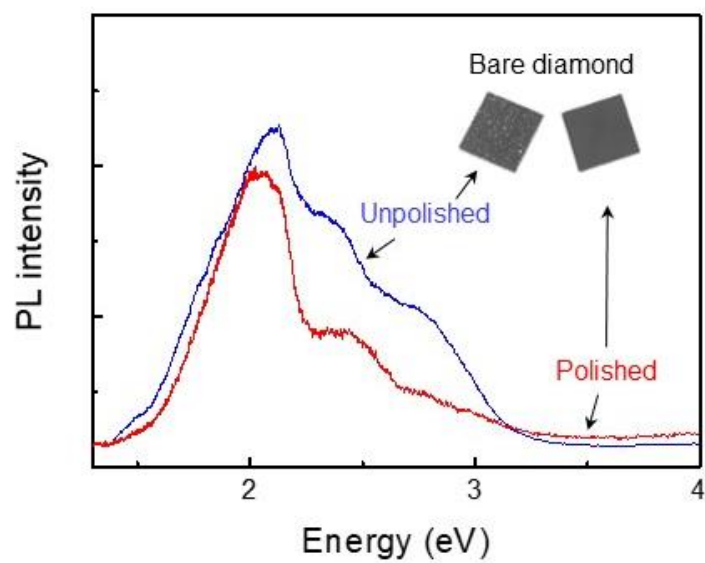


**Fig. S6.** Comparison of PL spectra of unpolished and polished bare diamond plates. They are those of Figure 5a and 5b, respectively. The  $\sim 2.69$  eV signal, analyzed in Figure 5b, decreases with polishing.

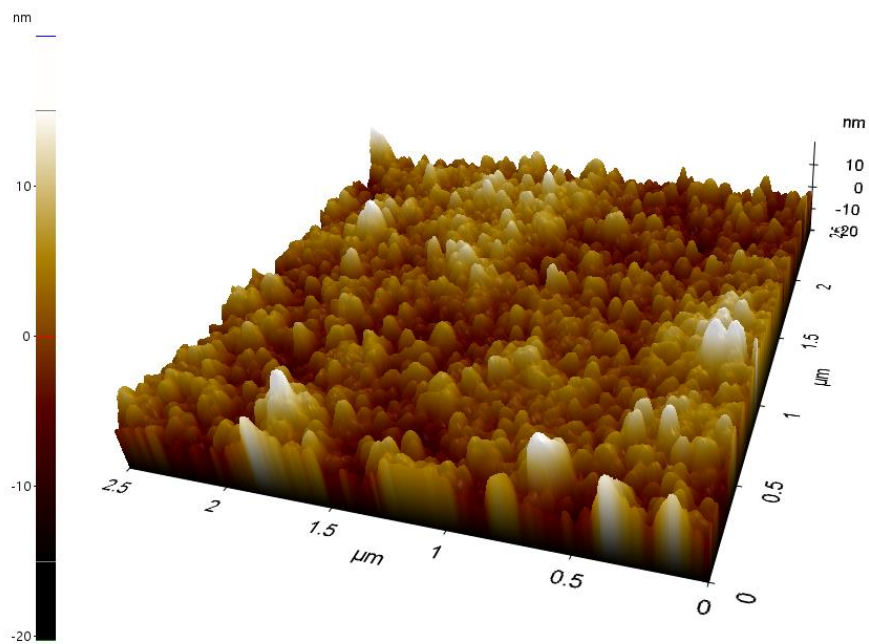


**Fig. S7.** AFM image obtained from the scrubbed (graphene side) face of the sample. The surface is relatively rough compared with that of as-grown for 1 min (Figure 2c) because the graphene layers were torn out by hand scrubbing. RMS was measured to be  $\sim 9$  nm.

## Absorption properties

Envisaging the potential application of the above geometry, we look for the optoelectronic properties. They are described by the complex dielectric function, *i.e.*  $\epsilon(\omega) = \epsilon_1(\omega) + i \epsilon_2(\omega)$ . The components of dielectric tensor are given by a sum of inter band and intra band contributions. The imaginary part of dielectric tensor  $\epsilon_2^{\alpha\beta}(\omega)$  is determined by summation over empty band as follows.

$$\epsilon_2^{\alpha\beta}(\omega) = \frac{2\pi e^2}{\Omega \epsilon_0} + \sum_{k,v,c} \delta((E^c_k - E^v_k - \hbar\omega)) | \langle \psi^c_k | u \cdot r | \psi^v_k \rangle |^2$$

where  $\epsilon_0$  is the vacuum dielectric constant,  $\Omega$  is the volume,  $v$  and  $c$  represent the valence and conduction bands respectively,  $\hbar\omega$  is the energy of the incident photon,  $u$  is the vector defining the polarization of the incident electric field,  $u \cdot r$  is the momentum operator, and  $\psi^c_k$  and  $\psi^v_k$  are the wave functions of the conduction and valence bands at the  $k$  point, respectively.

The absorption properties  $\alpha(\omega)$  can be calculated by the equation

$$\alpha(\omega) = \frac{\sqrt{2\omega}}{c} \{ [ \epsilon_1^2(\omega) + \epsilon_2^2(\omega) ]^{0.5} - \epsilon_1(\omega) \}^{0.5}$$

where  $\epsilon_1$  and  $\epsilon_2$  are the real and imaginary part of the complex dielectric function. The real part of the dielectric function can be written as

$$\epsilon_1^{\alpha\beta}(\omega) = 1 + \frac{2}{\pi} P \int_0^{\infty} \frac{\epsilon_2^{\alpha\beta}(\omega') \omega'}{\omega'^2 - \omega^2 + i\eta} d\omega'$$

where  $P$  is the principal value.

The pristine graphite with various stacking shows similar absorption peak. The prominent peak around 4.42 eV is due to  $\pi$ - $\pi^*$  (intra band) transition.<sup>45,46</sup> The high energy peaks for the graphene are  $\sigma$ - $\pi^*$  and  $\pi$ - $\sigma^*$  transitions. The peak for the diamond is due to  $\sigma$ - $\sigma^*$  transition. For the hybrid structure the visible range transition is mainly due to  $\pi$ - $\pi^*$  transition, which feels redshift, which be due to unique interface.

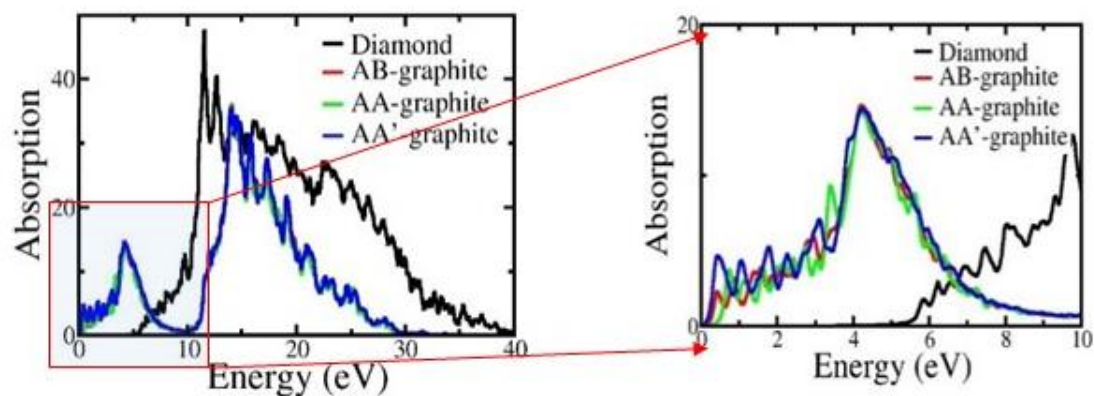


**Fig. S8.** Absorption spectra of pristine diamond, and graphite structures.

## References

40. P. Giannozzi, S. Baroni, N. Bonini, M. Calandra, R. Car, C. Cavazzoni, D. Ceresoli, G. L. Chiarotti, M. Cococcioni, I. Dabo, A. D. Corso, S. de Gironcoli, S. Fabris, G. Fratesi, R. Gebauer, U. Gerstmann, C. Gougousis, A. Kokalj, M. Lazzeri, L. Martin-Samos, N. Marzari, F. Mauri, R. Mazzarello, S. Paolini, A. Pasquarello, L. Paulatto, C. Sbraccia, S. Scandolo, G. Sclauzero, A. P. Seitsonen, A. Smogunov, P. Umari and R. M. Wentzcovitch, QUANTUM ESPRESSO: a modular and open-source software project for quantum simulations of materials, *J. Phys. Condens. Matter* 2009, **21**, 395502.
41. J. P. Perdew, K. Burke and M. Ernzerhof, Generalized Gradient Approximation Made Simple, *Phys. Rev. Lett.* 1996, **77**, 3865.
42. D. Vanderbilt, Soft self-consistent pseudopotentials in a generalized eigenvalue formalism, *Phys. Rev. B: Condens. Matter Mater. Phys.*, 1990, **41**, 7892.
43. H. J. Monkhorst and J. D. Pack, Special points for Brillouin-zone integrations, *Phys. Rev. B: Condens. Matter Mater. Phys.*, 1976, **13**, 5188.
44. M. Methfessel and A. T. Paxton, High-precision sampling for Brillouin-zone integration in metals, *Phys. Rev. B: Condens. Matter Mater. Phys.*, 1989, **40**, 3616.
45. A. B. Djuricic and E. H. Li, Optical properties of graphite, *J. Appl. Phys.* 1999, **85**, 7404.

46. L. Yang, J. Deslippe, C.-H. Park, M. L. Cohen and S. G. Louie, Excitonic Effects on the Optical Response of Graphene and Bilayer Graphene, *Phys. Rev. Lett.* 2009, **103**, 186802.